Density-functional-theory study of 13-atom metal clusters M_{13}, M=Ta–Pt

Min Zhang and René Fournier
Department of Physics, York University, Toronto, Ontario, Canada M3J 1P3
(Received 20 August 2008; revised manuscript received 20 January 2009; published 10 April 2009)

We report on the structures of six proposed global minima (GMs) of M_{13} clusters (M=Ta, W, Re, Os, Ir, and Pt) and 62 isomers that are within roughly 1 eV of the GM. The GM and isomers were obtained after several global optimization runs using a first-principles (Perdew-Burke-Enzerhof exchange-correlation) method to evaluate the energy. The GM and lowest-energy isomers can be described qualitatively as amorphous and compact for Ta, W, and Pt; quasicrystalline for Re; and cubic-prismatic for Os and Ir. The icosahedron is more than 1 eV above the GM in all cases, except 0.56 eV for Ta_{13}. The ground-state electronic configuration of the atoms is essential to understand structural trends in the clusters. Elements with a nearly closed-shell ground-state atom (W and Pt) produce many more low-energy cluster isomers than elements with partially filled d shells, and those isomers are generally compact and amorphous. Partially filled d shells in Os and Ir lead to strong directional bonding and many 90° angles between nearest neighbors. The predicted spin multiplicity of the GM is 2 (Ta_{13}), 1 (W_{13}), 6 (Re_{13}), 5 (Os_{13}), 4 (Ir_{13}), and 3 (Pt_{13}), and the spin multiplicity of all isomers within 0.5 eV of the GM is within ±2 of these values and is smaller than 6.

DOI: 10.1103/PhysRevA.79.043203 PACS number(s): 36.40.Mr, 31.10.+z, 61.46.Bc

I. INTRODUCTION

Transition-metal (TM) clusters have been the subject of many theoretical [1–17] and experimental [18–23] studies because of their role in catalysis and other fields of nanotechnology [24], and also because of fundamental questions arising from differences between clusters and bulk solids. Knowledge of the geometric structure of these clusters is crucial to understand their physical and chemical properties. But it is quite difficult to determine the structure of small clusters experimentally. Various levels of theory have been used to try predicting the structure of TM clusters. Empirical potentials are not always reliable for structure prediction because they typically neglect the directional nature of d-d interactions and quantum effects such as those arising from spin magnetism, orbital symmetry, and electronic shell closings. Structure prediction is also very challenging for *ab initio* methods because of the partly filled d shells and strong electron correlation. In this study, we performed structural global optimizations for six 13-atom 5d TM clusters (from Ta_{13} to Pt_{13}) using density-functional theory (DFT) [25] with the Perdew-Burke-Enzerhof (PBE) [26] exchange-correlation functional. We then analyzed the DFT results in terms of basic ideas in an effort to simplify the many, and often complex, geometric structures and their relative energies (REs).

Simple ideas lead to general predictions about cluster structure. One such idea is that, in small clusters, the surface energy is large relative to the total energy. Therefore, one expects a strong tendency toward cluster structures that minimize surface area. This principle seems to apply to some 13-atom metal clusters (Li [27], Y [28], Sc [7], Pd [29], and Al [30]), rare-gas clusters [31], and clusters described by empirical potentials such as the embedded atom method [32–34], glue model [35], and Sutton-Chen potential [36]. Another idea is that there is a strain energy associated with having unequal nearest-neighbor distances, therefore, a tendency to favor structures with a sharp first peak in the pair distribution function [37,38]. For large clusters, at least, one expects that these two structural principles are important and should give qualitatively correct predictions. For example, one predicts that structures should evolve with size from polytetrahedral (minimizing surface area) to fcc or hcp (minimizing strain). We wanted to check the validity of these principles for very small 13-atom 5d TM clusters by looking in detail at computed structures of the global minimum (GM) and low-lying isomers. As we will see, 5d metals have a tendency for directional bonding and 90° angles, and this stabilizes a wide variety of 13-atom structures that have large surface area.

II. COMPUTATIONAL METHODS

There are two essential aspects to our calculations: the way we calculate the energy for a given configuration of nuclei (by DFT) and the way we search the potential-energy surface (PES) for the lowest minima (global optimization).

A. DFT method

We use the PBE exchange-correlation functional implemented in the Vienna *ab-initio* simulation package (VASP) [39,40]. Plane-wave basis set and projector augmented wave (PAW) method [41,42] were used. Because the spin multiplicity of the transition-metal clusters is unknown, we required a full relaxation for all energy calculations. We used the smearing method of Methfessel-Paxton of order 1 [43] with a width ranging from 0.05 to 0.08 eV. Only the gamma point in the Brillouin zone was sampled. The box size is an important parameter: if the box is too large calculations are very costly, but if it is too small the accuracy is affected. After many tests, we chose a cubic box with a size of roughly 15 Å (more than twice a typical diameter for our clusters) for fixed geometry calculations. For calculation of forces, and local geometry optimizations, the box size was set to 18 Å, and higher numerical accuracy was specified with these VASP keywords: PREC=high, EDIFF=10^{-7}, and EDIFFG=10^{-5}.

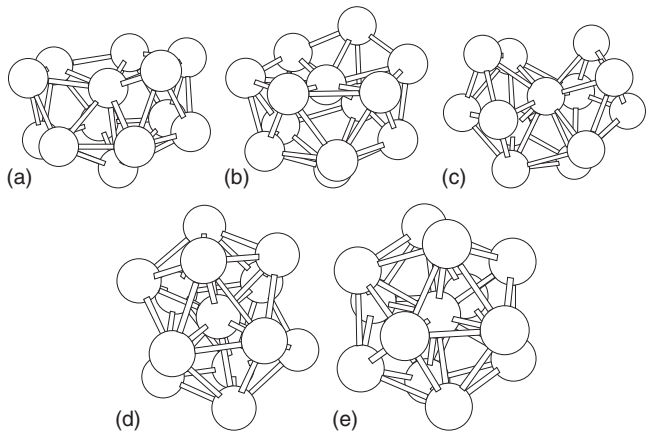

FIG. 1. (a)–(e) Isomers of Ta_{13} that are within 0.6 eV of the GM, in order of increasing energy (see Table I).

B. Global optimization

We used two very different global optimization algorithms: simulated annealing (SA) [44,45] and Tabu search in descriptors space (TSDS) [46]. Generally speaking, SA is time consuming. But it has no built-in bias, and with a slow enough cooling schedule it has a high probability of finding the GM [47]. The TSDS method, on the other hand, is very efficient because it uses descriptors to achieve a kind of dimensionality reduction and samples the PES in a discrete manner [46]. However, the choice of descriptors and sampling method in TSDS can introduce some biases and one runs the risk of missing the GM: this happened, for instance, for the 38-atom cluster of the Lennard-Jones potential [46]. By using *both methods*, and sometimes doing multiple runs, we feel that we have a very good chance of finding the GM and many of the low-lying isomers. We collected structures produced during the various SA and TSDS runs, performed local optimizations on them, and ended up with many distinct extrema of the PES. The lowest-energy structure found in each case will be referred to as the GM. We are also interested in low-lying isomers, mainly those within 1 eV or so of the GM.

We now introduce the types of structures involved, how we found them, and the way we label them. The icosahedron is a logical candidate for any 13-atom cluster: we label it "s1." In most cases we did multiple runs of SA and TSDS. Each run produces one GM candidate which we denote with a name starting with "s." Aside from that, we collected various proposed 13-atom cluster structures from the literature [1–4]. We label these with names starting with "t." The suffix "m" means the structure was modified somehow: t1m and t8m are modified versions of t1 and t8. We did local optimization on all of the s-type and t-type structures for every element. For instance, if a SA run on W_{13} produced a GM candidate "sn," then this sn structure was used as a starting point for a local optimization of W_{13} *and was used also*, after appropriate scaling of nuclear coordinates, for Ta_{13}, Re_{13}, Os_{13}, Ir_{13}, and Pt_{13}. The same goes for the t series of structures, so the s and t series are shared by all six M_{13} species. In addition, each M_{13} has structures that are unique to it and which we label simply by a number: they are low-energy isomers found by automated search of distinct structures among the large sample set generated during global optimization for that M_{13} cluster species. For each structure local optimization was done with different spin multiplicities to find the ground state. Local minima were then ranked by energy: the lowest one was accepted as the GM of M_{13} only if it had been generated by global optimization of *this* M_{13} species. Otherwise, we performed further global optimizations for this M_{13} species. The vibrational frequencies were calculated in all cases to make sure they are minima.

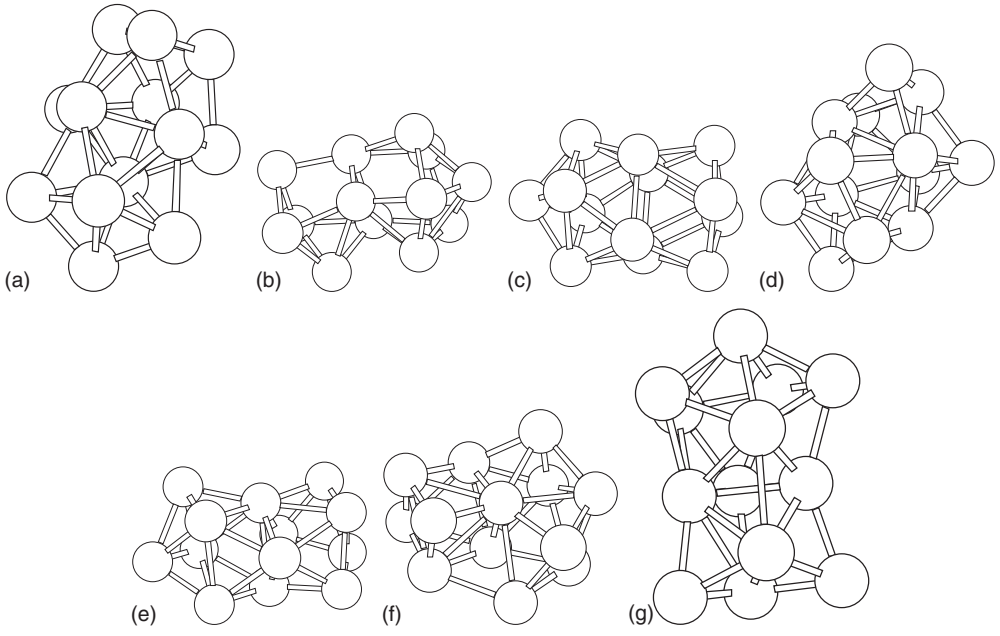

FIG. 2. (a)–(g) Isomers of W_{13} that are within 0.6 eV of the GM, in order of increasing energy (see Table II).

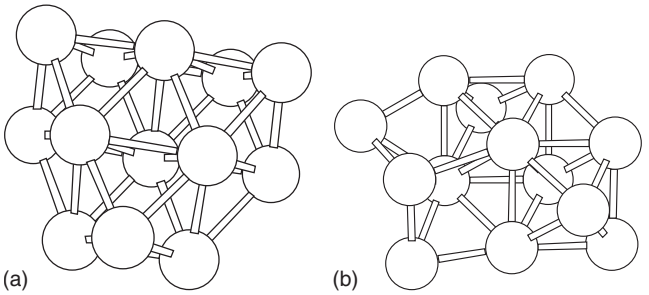

FIG. 3. (a) and (b) Isomers of Re_{13} that are within 0.6 eV of the GM, in order of increasing energy (see Table III).

III. RESULTS

The six GM structures that we found [48] have a lower VASP-PBE energy than other published structures. They are the first structures in Figs. 1–6 and the first entries in Tables I–VI: s3-B of Ta_{13}, s13-A of W_{13}, s9-E of Re_{13}, s5-D of Os_{13}, s10-D of Ir_{13}, and s12-B of Pt_{13}. We also found 62 isomers within 1.15 eV of the GM. The REs and a few other properties are reported in Tables I–VI for those 68 structures, and their Cartesian coordinates can be found elsewhere [49]. We have shown only a subset of 36 structures in Figs. 1–6, those within 0.6 eV of the GM; however, we used the full set of 68 structures for analysis (Sec. III B). The principle of surface-energy minimization suggests the icosahedron as the GM for all six 13-atom 5*d* TM clusters. In fact, the icosahedron is favored in none of these clusters and it has a high energy relative to the GM in all cases: +0.56 eV for Ta_{13}, +1.60 eV for W_{13}, +3.89 eV for Re_{13}, +6.22 eV for Os_{13}, +6.49 eV for Ir_{13}, and +3.31 eV for Pt_{13}. Based on these energy differences, we feel very confident that the icosahedron is not the GM for any of these M_{13} metal clusters and is not relevant for thermally averaged properties, with the possible exception of Ta_{13}. In order to check the effect of exchange correlation, we repeated local optimizations in the local-density approximation (LDA) [50–53] for s and t series. We found no significant changes in the RE of the icosahedron and GM in going from PBE to LDA. We also calculated the zero-point energy (ZPE) correction and the Gibbs free energy at 298 K with the usual approximations [54] for all 68 isomers. These results are in Tables I–VI. The ZPE and estimated contributions from entropy make only very small changes to the RE and the same GM persists.

A. Properties of global minima

One can never be sure that the GM of a cluster has been found. More accurate energy calculations could change RE

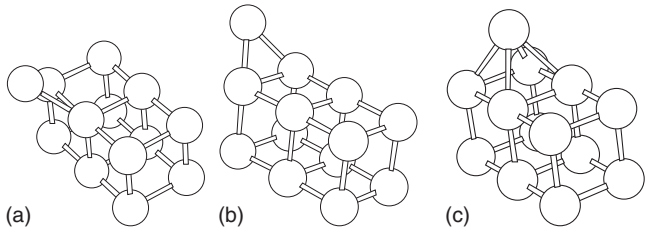

FIG. 5. (a)–(c) Isomers of Ir_{13} that are within 0.6 eV of the GM, in order of increasing energy (see Table V).

of isomers by possibly a few tenths of an eV. Therefore, it is important to look not only at the GM but also at low-lying isomers, and it is useful to identify similarities and differences between structures within an M_{13} species, or in cross comparison, e.g., comparing low-energy structures of Ta_{13} to low-energy structures of W_{13}. There is obviously a wide variety of structural isomers (see Figs. 1–6 and supplementary material [49]). Many of them have a complicated low-symmetry geometry. It is difficult to grasp similarities or differences by simply looking at pictures of isomers. In order to characterize structures in some detail, we analyzed the distribution of angles θ_{ijk} formed by nearest neighbors i and k of some atom j. We consider atoms i and j to be nearest neighbors when $d_{ij} < 1.2 \min\{d_{ik} | k=1,\ldots,N \text{ and } k \neq i\}$. The discrete set of those angles was then replaced with a sum of narrow Gaussians to produce a continuous distribution. Peaks at 90°, 108°, and 120° are normally due to rectangles, pentagons, and hexagons. Generally, these peaks could be indicative of hybridized atomic states (e.g., $sp^3 = 109.5°$ and $sp^2 = 120°$). The width and relative height of peaks are very helpful for classifying structures. For example, sharp peaks signal crystal-like structures while broad distributions are typical of amorphous structures; polytetrahedral (or icosahedral) structures have many 60° angles, whereas prismatic or cubic structure obviously have many 90° angles.

The angle distributions for the six GMs are shown in Fig. 7(a). The most interesting observation is the trend in the 90° angle peak. The distribution for Ir_{13} is essentially a single sharp peak at 90°, and indeed Ir_{13} has a crystal-like structure built from rectangles [see Fig. 5(a)]. Likewise, the Os_{13} angle distribution has a prominent peak near 90°, but it also has some angles close to 60° [see Fig. 4(a)]. In going from Os_{13} to Re_{13}, the density around 90° falls and density near 60° and 120° rises. As we go further left in the periodic table, to W_{13} and Ta_{13}, the density near 90° keeps decreasing to essentially zero, and simultaneously the distribution spreads out. So, in going from Re_{13} to Ta_{13} the number of right angles in the

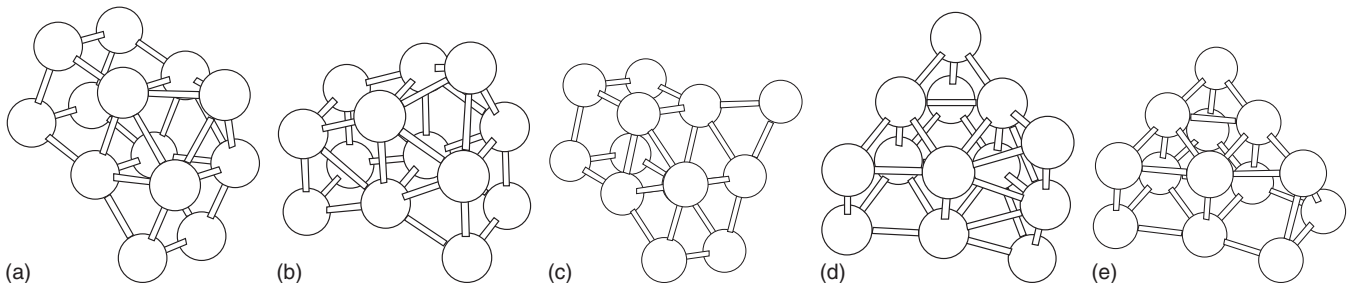

FIG. 4. (a)–(e) Isomers of Os_{13} that are within 0.6 eV of the GM, in order of increasing energy (see Table IV).

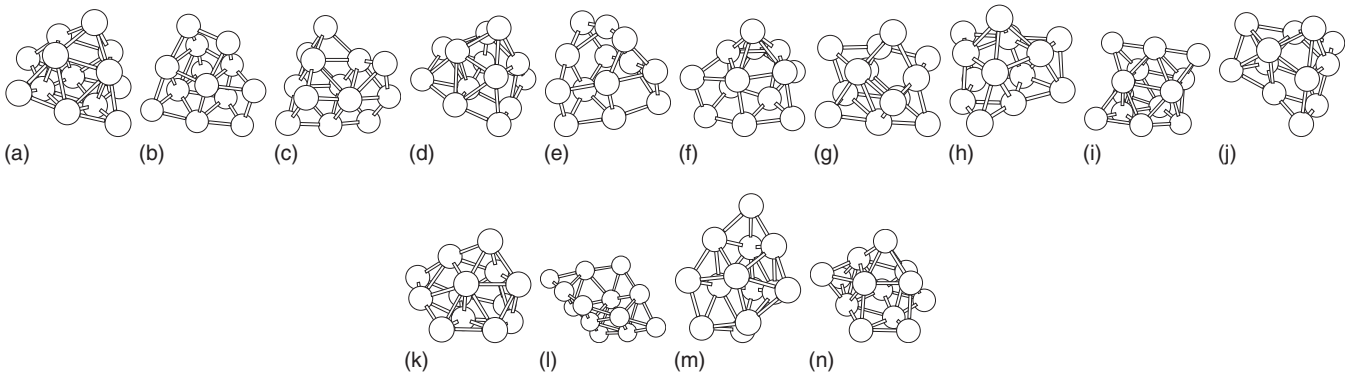

FIG. 6. (a)–(n) Isomers of Pt_{13} that are within 0.6 eV of the GM, in order of increasing energy (see Table VI).

GM decreases and the structure becomes more amorphous. This can also be seen from Figs. 1(a), 2(a), and 3(a). If we go to the right of Ir in the periodic table, to Pt_{13}, we see something similar but more dramatic. The peak around 90° nearly vanishes, the density in the distribution moves to 60°, and it spreads out a lot [see also Fig. 6(a)]. Interestingly, we see essentially the same trends across the 5*d* series if we average the angle distributions of *all* the low-lying isomers of a given element. This is shown in Fig. 7(b). In other words, iridium has a general tendency to adopt 13-atom structures with many 90° angles, tungsten has a general tendency to adopt amorphous 13-atom structures, etc. There must be an explanation for this rooted in the properties of those elements. We will now address this point.

The *d* orbitals play an important role in bonding of TMs. These orbitals are directional and perpendicular to each other. It seems logical that *d*-*d* bonding in TM clusters would favor 90° angles in low-energy structures. The density of states (DOS) decomposed into *s*, *p*, and *d* contributions shows that *d* bonding is prominent in all six cases. Yet, *d* bonding does not produce 90° angles in Ta_{13}. We looked at a few electronic properties and found that two of them could explain the observed trend.

The first one is localization. More localized *d* orbitals imply stronger directional bonds which ideally should be perpendicular to each other. To verify this, we did natural bond orbital (NBO) analysis [55] for all GMs. The degree of localization is measured by the percentage of valence orbitals that are of "Lewis valence" type. These values, listed in Table VII from Ta to Pt, show increasing localization as one would expect from the increasing effective nuclear charge. The GM of Ta_{13} has the least localized orbitals (see Table VII) and has a compact amorphous structure. The degree of localization is very similar among W_{13}, Re_{13}, and Os_{13}, and is much higher than for Ta_{13}. But W_{13} and Re_{13} have very

TABLE I. Isomers of Ta_{13}, their relative energy (RE), multiplicity, zero-point energy, and relative Gibbs free energy (RG). The lowest calculated VASP energy (for s3-B) is −124.45 eV. The suffixes -A, -B, -C, -D, and -E indicate CA group membership (see Sec. III B 2) and structures are depicted in Fig. 1.

Index	RE (eV)	$2S+1$	ZPE (eV)	RG (eV)
s3-B	0.00	2	0.29	0.00
8-B	0.18	2	0.28	0.15
t5-A	0.24	2	0.28	0.15
t0-A	0.46	2	0.26	0.25
s1-C	0.58	4	0.25	0.43
14-C	0.79	2	0.28	0.76

TABLE II. Isomers of W_{13}. The meaning of symbols is like in Table I and geometric structures are depicted in Fig. 2. The lowest calculated VASP energy (for s13-A) is −131.18 eV.

Index	RE (eV)	$2S+1$	ZPE (eV)	RG (eV)
s13-A	0.00	1	0.32	0.00
33-A	0.26	1	0.31	0.23
30-C	0.32	3	0.31	0.29
6-C	0.49	1	0.31	0.49
t2-A	0.51	1	0.31	0.50
27-B	0.56	3	0.31	0.51
t0-A	0.59	1	0.31	0.54
4-B	0.66	1	0.31	0.61
t1m-B	0.70	1	0.31	0.64
3-C	0.70	1	0.31	0.68
14-E	0.71	3	0.31	0.64
16-A	0.72	3	0.31	0.70
7-B	0.76	1	0.30	0.70
18-A	0.77	1	0.32	0.76
29-A	0.77	1	0.31	0.72
s8-E	0.78	1	0.30	0.72
5-A	0.80	1	0.31	0.77
10-A	0.87	3	0.30	0.79
t1-A	0.93	3	0.30	0.81
26-B	0.94	1	0.30	0.87
20-A	0.96	1	0.30	0.88
8-A	0.98	3	0.31	0.93
s3-B	1.01	3	0.30	0.93
s4-B	1.07	3	0.30	0.97
12-B	1.15	1	0.30	1.08

TABLE III. Isomers of Re_{13}. The meaning of symbols is like in Table I. and geometric structures are depicted in Fig. 3. The lowest calculated VASP energy (for s9-E) is −126.36 eV.

Index	RE (eV)	$2S+1$	ZPE (eV)	RG (eV)
s9-E	0.00	6	0.32	0.00
s11-E	0.43	4	0.32	0.40
s4-B	0.85	4	0.31	0.81
15-A	0.97	2	0.32	0.98

few right angles while Os_{13} has many. We need something else to explain this difference.

The second factor is the electronic structure of the atoms Ta–Pt, which are, after all, the building blocks for the clusters. The orbital energies of the ground-state atoms calculated with PBE are shown in Table VIII. The W and Re atoms have a similar pattern of orbital energies: a half-filled *d* shell with occupied *d* spin-up orbitals and empty *d* spin-down orbitals. The spin-up *d* orbitals all have the same energy. So the *d* shell produces a spherical electron density and a set of five equivalent *d*-type spin orbitals. This essentially removes the directional attribute of *d* orbitals. There is a big energy gap between spin-up and spin-down orbitals, making it energetically costly to promote electrons from one spin manifold to the other, break the symmetry, and "prepare" W or Re atom for directional bonding. That is why we do not find many right angles in W_{13} and Re_{13}. The Os atom has very different orbital energies. Its electronic configuration is d^5 for spin up and d^1 for spin down, and there are many low-lying nonspherical electronic configurations. This allows preferential bond formation along certain directions. Of course, a proper treatment of any atom must give a spherical electron density. But the point is that the gap between occupied and virtual *d* spin orbitals is small, so the Os atom *d* shell can be polarized easily. In the language of orbital theory, the energy cost for exciting electrons from occupied to virtual orbitals is small in Os, but large in W and Re. It implies that an Os atom with an asymmetric distribution of neighbors can easily be promoted to an electronic configuration that satisfies directional bonding requirements. This explains why Os_{13} has many more right angles than W_{13} and Re_{13}.

TABLE IV. Isomers of Os_{13}. The meaning of symbols is like in Table I and geometric structures are depicted in Fig. 4. The lowest calculated VASP energy (for s5-D) is −109.75 eV.

Index	RE (eV)	$2S+1$	ZPE (eV)	RG (eV)
s5-D	0.00	5	0.34	0.00
5-D	0.40	5	0.33	0.40
s10-D	0.44	5	0.34	0.43
s7-C	0.56	1	0.33	0.60
s4-C	0.57	5	0.33	0.53
24-D	0.81	3	0.33	0.80
29-D	0.82	3	0.33	0.82

TABLE V. Isomers of Ir_{13}. The meaning of symbols is like in Table I and geometric structures are depicted in Fig. 5. The lowest calculated VASP energy (for s10-D) is −86.57 eV.

Index	RE (eV)	$2S+1$	ZPE (eV)	RG (eV)
s10-D	0.00	4	0.33	0.00
t10-D	0.25	4	0.33	0.26
t0-D	0.27	4	0.32	0.27
t2-D	0.92	8	0.31	0.83
s5-D	1.01	2	0.32	1.00
s6-D	1.03	2	0.31	1.00

The Ir atom *d* shell is similar to that of Os—small gap between occupied and unoccupied *d* orbitals and different energies within each spin *d* manifold. But the Ir atom has one more spin-down *d* electron, so it is further away from the symmetric *d* shell of W and Re. Also, bonds are more localized in Ir_{13} than in Os_{13} (Table VII). These two things explain why Ir has a stronger tendency to form rectangles than Os. The GM of Pt_{13} has the highest degree of orbital localization, yet it has few 90° angles (just one square). Again, the reason for this can be found in the electronic configuration of the Pt atom, $5d^96s^1$. The *d* orbitals are very close in energy, and there is *s*-*d* hybridization which gives the Pt atom a nearly closed (and symmetric) *d*-shell character.

The trend in atomization energy (AE) of GMs, shown in Table VII, is consistent with this analysis. The Ta_{13} cluster

TABLE VI. Isomers of Pt_{13}. The meaning of symbols is like in Table I and geometric structures are depicted in Fig. 6. The lowest calculated VASP energy (for s12-B) is −57.31 eV.

Index	RE (eV)	$2S+1$	ZPE (eV)	RG (eV)
s12-B	0.00	3	0.24	0.00
t6-B	0.19	3	0.24	0.12
s6-C	0.23	3	0.25	0.24
s8-C	0.23	3	0.24	0.21
s7-C	0.25	3	0.25	0.23
29-C	0.33	1	0.24	0.33
t1-B	0.40	5	0.24	0.34
9-C	0.42	1	0.24	0.40
25-C	0.45	3	0.24	0.44
s2-C	0.49	5	0.24	0.42
22-C	0.51	7	0.23	0.42
6-A	0.52	1	0.24	0.53
21-A	0.53	1	0.23	0.51
17-B	0.54	5	0.24	0.49
s4-D	0.76	1	0.25	0.77
11-A	0.79	3	0.23	0.74
5-C	0.86	1	0.24	0.86
15-C	0.94	3	0.23	0.89
2-A	0.95	3	0.23	0.91
4-C	1.00	5	0.22	0.89

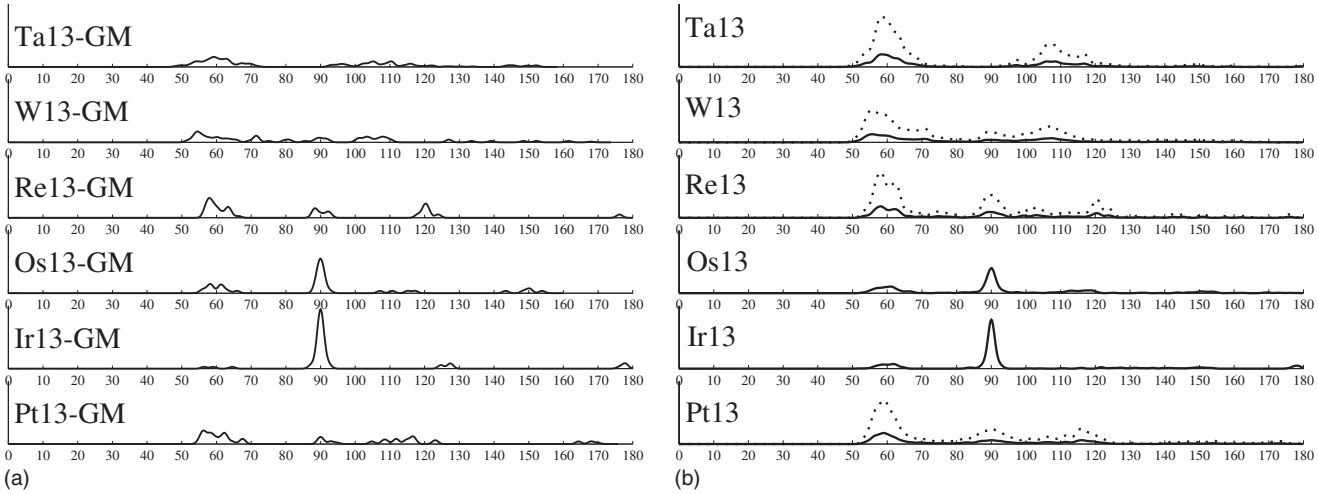

FIG. 7. (a) and (b) Angle distributions for the 13-atom 5*d* transition-metal clusters.

has the most delocalized bonding and smallest effective nuclear charge: this increases overlap between *d* orbitals which helps achieve a high AE, and it also disfavors directional bonding, which produces a compact but amorphous structure. The 13-atom clusters of W and Re have relatively small 13-atom cohesive energies despite a high bulk cohesive energy. We think this is due to the half-filled and symmetric closed-shell character of their atomic *d* orbitals. This atomic electronic configuration is not favorable when most atoms have an anisotropic distribution of nearest neighbors as is the case in small clusters. The relatively low AE of Pt_{13} is due to its nearly closed *d* shell. Other factors, for example *s*-*d* hybridization, may play a role in determining trends in structure and AE of 13-atom 5*d* TM clusters. However, the *s*, *p*, and *d* projected DOSs of the six GMs (they are not shown here but can be found in the supplementary material [49]) do not show any simple features that would relate to the favored geometric structures. We believe that orbital localization and the ground-state electronic structure of the atoms give the simplest explanations for these trends. We calculated the vertical ionization energy (VIE) and vertical electron affinity (VEA) (see Table VII). The VIE and VEA both increase from left to right as we expect based on the increasing effective nuclear charge.

TABLE VII. Calculated properties of the global minima. Vertical electron affinity (VEA), vertical ionization energy (VIE), atomization energy per atom (AE), and the ratio of electron populations [(Lewis valence)/(Valence)], which is a measure of electron localization.

	VEA (eV)	VIE (eV)	AE (eV/atom)	Lewis valence / Valence
Ta_{13}	1.65	4.83	5.97	0.68
W_{13}	1.79	4.94	5.43	0.77
Re_{13}	2.41	5.59	5.12	0.78
Os_{13}	2.73	6.00	5.52	0.78
Ir_{13}	2.92	6.37	5.17	0.83
Pt_{13}	3.05	6.64	3.85	0.90

B. Low-energy isomers

The GM only gives information about the lowest point on the PES. For a better understanding, we need to look at other important points of the clusters' PES. We searched the sample sets generated by the global optimization calculations for each cluster to find low-energy (RE$<$1 eV) isomers. For W_{13} and Ir_{13}, we included a few isomers whose REs are slightly higher than 1 eV. Note that all these isomers are locally optimized and their vibrational frequencies confirm that they are minima. Only isomers with RE$\leq$0.6 eV are shown in Figs. 1–6, but the following analysis is based on the set of isomers having RE$\leq$1.15 eV [49].

1. Energy of isomers

There are 68 isomers in total, including the GM, for the six 13-atom clusters. It is interesting that for W_{13} and Pt_{13} we discovered a very large number of isomers, 25 and 20, respectively. For the other elements we found no more than ten isomers. It is unlikely that we missed many low-lying isomers for Ta, Re, Os, and Ir, but not W and Pt: we did SA and TSDS searches in all six cases. As for the trend in 90° angles discussed earlier, the electronic structure of the atoms is a key to understand why there are more isomers of W_{13} and Pt_{13}. Both W and Pt are almost spherical, W with half-filled *d* shell and Pt with nearly filled *d* shell, and show little evidence of directional bonding. This means that angle deformations that transform an isomer into another isomer should produce relatively small energy changes resulting in numerous low-lying isomers. The Os and Ir atoms, on the contrary, have a strong preference for 90° angles. So most angle deformations that transform one isomer into another will be accompanied by energy changes higher than 1 eV, i.e., fewer low-lying isomers. The case of Re is more subtle. Unlike W, the Re atom has an occupied spin-down *s* atomic orbital that is not far below the unoccupied spin-down *d* orbitals. The excitation energy required to break the *d*-shell symmetry is roughly 1.5 eV in the Re atom (*s*-*d* excitation) compared to roughly 3.2 eV in the W atom (*d*-*d* excitation). This accounts for the fact that the number of 90° angles in Re_{13} is intermediate between W_{13} and Os_{13}. This would also explain why

TABLE VIII. Energy, type, and occupancy (occu.) of spin orbitals calculated by PBE for the ground state of the atoms Ta–Pt. (a) *s-d* hybrid having 16% *s* character and (b) *s-d* hybrid having 59% *s* character.

Ta			W		
E (eV)	Spin	Occu.	*E* (eV)	Spin	Occu.
−5.6	$s\uparrow$	1/1	−5.6	$s\uparrow$	1/1
−4.6	$s\downarrow$	1/1	−4.0	$d\uparrow$	5/5
−4.4	$d\uparrow$	1/1	−2.4	$s\downarrow$	0/1
−4.0	$d\uparrow$	2/2	−1.3	$p\uparrow$	0/3
−3.8	$d\uparrow$	0/2	−0.7	$d\downarrow$	0/5
−2.9	$d\downarrow$	0/2	−0.3	$s\uparrow$	0/1
−2.3	$d\downarrow$	0/1			
−1.9	$d\downarrow$	0/2			
−1.4	$p\uparrow$	0/2			
−1.0	$p\downarrow$	0/1			
−0.7	$p\downarrow$	0/1			
Re			Os		
E (eV)	Spin	Occu	*E* (eV)	Spin	Occu.
−6.4	$s\uparrow$	1/1	−7.2	$d\uparrow$	3/3
−6.3	$d\uparrow$	5/5	−7.0	$d\uparrow$	1/1
−4.7	$s\downarrow$	1/1	−6.5	$s\uparrow$	1/1
−3.4	$d\downarrow$	0/5	−6.3	$d\uparrow$	1/1
−1.4	$p\uparrow$	0/3	−5.1	$s\downarrow$	1/1
−0.7	$p\downarrow$	0/3	−4.9	$d\downarrow$	1/1
−0.1	$s\uparrow$	0/1	−4.7	$d\downarrow$	0/1
−0.0	$s\downarrow$	0/1	−4.5	$d\downarrow$	0/2
			−3.9	$d\downarrow$	0/1
Ir			Pt		
E (eV)	Spin	Occu.	*E* (eV)	Spin	Occu.
−7.8	$d\uparrow$	2/2	−7.3	$d\uparrow$	1/1
−7.5	$d\uparrow$	1/1	−6.5	$d\uparrow$	1/1
−7.0	$d\uparrow$	1/1	−6.3	$sd\uparrow$(a)	1/1
−6.8	$d\uparrow$	1/1	−6.2	$d\uparrow$	2/2
−6.4	$s\uparrow$	1/1	−6.0	$d\downarrow$	1/1
−6.0	$d\downarrow$	1/1	−5.9	$sd\uparrow$(b)	1/1
−5.8	$d\downarrow$	1/1	−5.5	$d\downarrow$	2/2
−5.3	$s\downarrow$	1/1	−5.3	$d\downarrow$	1/2
−5.3	$d\downarrow$	0/1	−5.0	$s\downarrow$	0/1
−5.2	$d\downarrow$	0/2			

Re_{13} has fewer low-lying isomers than W_{13}, but it is unclear why Re_{13} has so few isomers (fewer than Os_{13}). Tantalum is also an intermediate case: electrons are highly delocalized in Ta_{13}, but the Ta atom electronic configuration is nonspherical as for Os and Ir. This apparently manifests itself in Ta_{13} having few low-energy isomers with structures that are neither cubic (like Os or Ir) nor amorphous (like W or Pt).

TABLE IX. Average values of descriptors and relative energies for each group of structural isomers.

Group	*d*1	*d*2	*d*5	*d*6	*P*(60°)	*P*(90°)	RE (eV)
A	5.31	1.34	0.19	0.36	0.07	0.02	0.66
B	5.26	1.60	0.08	−0.03	0.06	0.02	0.60
C	4.86	1.20	0.04	−0.01	0.11	0.05	0.54
D	3.80	0.89	0.14	0.17	0.04	0.31	0.56
E	5.39	1.58	0.13	−0.18	0.10	0.04	0.48

2. Classifying the isomers

There are many isomers, and it is not fruitful to analyze the structure of each one. Instead, we seek to get overall information by applying statistical methods to the set of 68 structures in Fig. 1–6. Our approach is to first classify the isomers by cluster analysis (CA) [56]. Then, we calculate averages for properties of interest for each group that was identified by the CA. By comparing groups of isomers, we get a better sense for what is similar or different between elements. This, in effect, is a comparison of some essential aspects of the clusters PES. In order to perform CA for isomers, we start by representing them with several descriptors. The first four descriptors we choose are part of the set used in the TSDS optimization itself: the mean coordination *d*1, the root-mean-square (RMS) deviation of atomic coordinations *d*2, the asphericity *d*5 which ranges between 0 and 1, and the shape *d*6 which ranges between −0.5 and 1. Descriptors *d*5 and *d*6 are calculated from moments of inertia [46]. A negative value of *d*6 means the shape is oblate while a positive value means that it is prolate. Two descriptors related to the angle distribution also appear to be important: the probabilities of an angle in a cluster to be close to 60° [*P*(60°)] and 90° [*P*(90°)]. By "close" we mean that an angle is within 1° of that value. These two descriptors emphasize the local aspects of structure.

For the CA we chose standard procedures from the SAS suite of routines. First, the six-dimensional data set with 68 members is transformed to a new set of six variables by the procedure *ACECLUS* (see Chap. 16 of SAS guide [57]) that make the within-cluster covariance matrix spherical. Then we classify the transformed data by procedure *CLUSTER* (see Chap. 23 of SAS guide [57]). After many tests, we chose the two-stage density linkage [57] method. The set of 68 isomers was classified into five groups: A, B, C, D, and E. The relevant results are summarized in Tables IX and X. In Figs. 1–6 and Tables I–VI, the suffix in the label of each isomer shows its group membership. One way to visualize the structural groups is to name them according to the following attributes: *amorphous* [small value of $P(90°)+P(60°)$], *quasicrystalline* [large $P(90°)+P(60°)$], *prismatic* [large $P(90°)-P(60°)$], *spherical* (small $d5+|d6|$), *prolate* (large $d5+d6$), and *oblate* (large $d5-d6$). Thus, we call group A the amorphous prolate group, B the amorphous spherical group, C quasicrystalline spherical, E quasicrystalline oblate, and D the prismatic group.

Group A is composed mostly of isomers of the spherical atoms, W_{13} (63%) and Pt_{13} (21%). Isomers of group B have

TABLE X. Composition of isomer groups by element. Each cell contains four data which can be explained with an example, e.g., (Ta, group A). There are 2 Ta_{13} isomers in group A, which amounts to 3% of all isomers, 11% of all group A isomers, and 33% of all Ta_{13} isomers. The "total" column and row are a sum of the "frequency" and "percent" in that row and column, respectively.

Frequency Percent Row pct. Col. pct. Group	Element						
	Ta	W	Re	Os	Ir	Pt	Total
A	2	12	1	0	0	4	19
	0.03	0.18	0.01	0.00	0.00	0.06	0.28
	0.11	0.63	0.05	0.00	0.00	0.21	
	0.33	0.48	0.25	0.00	0.00	0.20	
B	2	8	1	0.00	0.00	4	15
	0.03	0.12	0.01	0.00	0.00	0.06	0.22
	0.13	0.53	0.07	0.00	0.00	0.27	
	0.33	0.32	0.25	0.00	0.00	0.20	
C	2	3	0	2	0.00	11	18
	0.03	0.04	0.00	0.03	0.00	0.16	0.26
	0.11	0.17	0.00	0.11	0.00	0.61	
	0.33	0.12	0.00	0.29	0.00	0.55	
D	0	0	0	5	6	1	12
	0.00	0.00	0.00	0.07	0.09	0.01	0.18
	0.00	0.00	0.00	0.42	0.50	0.08	
	0.00	0.00	0.00	0.71	1.00	0.05	
E	0	2	2	0	0	0	4
	0.00	0.03	0.03	0.00	0.00	0.00	0.06
	0.00	0.50	0.50	0.00	0.00	0.00	
	0.00	0.08	0.50	0.00	0.00	0.00	
Total	6	25	4	7	6	20	68
	0.09	0.37	0.06	0.10	0.09	0.29	1.00

nearly the same element-by-element breakdown as group A. Group C consists mostly of Pt and W clusters, like groups A and B, but it is Pt rich instead of W rich: W_{13} (17%) and Pt_{13} (61%). Of course we did not use the atomic number as a variable in the analysis, so the different W and Pt contents between groups A and C reflect true differences in the structures that these two elements tend to adopt. Examining Table X, we can also see that Re_{13} is more like W_{13} than like Pt_{13}. The smaller $d1$ (coordination number) of group C isomers is related to the higher average $P(60°)$ and $P(90°)$. In the definitions of these probabilities we set a strict tolerance ($\pm 1°$) for counting in an angle. So the very small $P(60°)$ and $P(90°)$ in groups A and B show that geometries are distorted away from equilateral triangles and perfect rectangles. This correlates with more compact structures and higher coordination numbers. Groups A–C are composed mainly of W_{13} and Pt_{13} isomers partly because of the much larger number of isomers for these two elements: all six of Ta_{13} belong to group A, B, or C (two Ta_{13} isomers each), so in a sense Ta is also an important contributor to those groups. But the element composition of groups A–C also reflect a similarity in electronic structure of the W and Pt atoms (and to a lesser extent, Re and Ta atoms). Group D is formed almost purely by Ir_{13} (42%) and Os_{13} (50%) isomers. Group E is the smallest group with only four members, two W_{13} (14-E and s8-E) and two Re_{13} (s9-E and s11-E) isomers. The similarity in the electronic structures of the W and Re atoms may explain why a group made of only W_{13} and Re_{13} isomers is created by the CA. However the number of isomers in this group is too small to draw a firm conclusion. In summary, the tendency for isomers of different elements to fall in a common structural group, e.g., W-Pt, Os-Ir, and W-Re, shows that there are similarities between the PES of these clusters rooted in the electronic structures of their constituent atoms. The last column of Table IX shows that there is no correlation between groups and RE.

There is a lot of freedom in how one can choose descriptors or carry out a CA, and our choices are maybe not the best. But with these choices we could find groups of isomers that display consistent trends. Generally, we believe that some sort of classification or statistical analysis is necessary for understanding structure in cases, like here, where many cluster isomers have comparable energies. As another example of how CA can be used to find periodic trends, we took the first entries in Table X of each element to form vectors, such as (2,2,2,0,0) for Ta, as a way to summarize the

M_{13} cluster structure characteristics of each element. We took scalar products $[\vec{a}\cdot\vec{b}/(ab)]$ of these vectors to express structural similarity between different elements. By that measure, the most similar pairs of elements, with their scalar products in parentheses, are Os-Ir (0.93), Ta-W (0.89), Ta-Pt (0.88), W-Re (0.66), and W-Pt (0.61). The least similar pairs have a zero scalar product: Re-Os, Ta-Ir, W-Ir, and Re-Ir.

IV. CONCLUSION

We have found GMs for six 13-atom 5*d* TM clusters, Ta_{13}-Pt_{13}, by global optimization with two different algorithms and an energy calculated from first principles (DFT-PBE). None of these GM is an icosahedron. We advocate using the distribution of angles for analyzing the structure of cluster isomers. We found a trend in the number of 90° angles as we go across the Ta-Pt series, with maximum right angles for Os and Ir. We explained this on the basis of two things: orbital localization and electronic structure of the constituent atoms. To get more general information about the PES of these 13-atom clusters, we looked at the set of 68 low-energy (within 1 eV of GM roughly) structural isomers of the six cluster species as a whole. Surprisingly, the number of isomers we discovered varies a lot according to element: Ta (6 isomers), W (25), Re (4), Os (7), Ir (6), and Pt (20). Atomic orbital energies and configurations explain these differences: atoms with a spherical or nearly spherical ground-state electronic configuration (W and Pt) have many low-energy isomers and atoms with nonspherical ground-state electronic configurations have fewer isomers. We used a cluster analysis algorithm to analyze the set of 68 cluster structures and found that they fall into five groups. Elements with similar atomic electronic structure tend to produce similar cluster isomers.

ACKNOWLEDGMENT

This work was made possible by the facilities of the Shared Hierarchical Academic Research Computing Network (SHARCNET) [58].

[1] L. Xiao and L. Wang, J. Phys. Chem. A **108**, 8605 (2004).
[2] E. Aprà and A. Fortunelli, J. Phys. Chem. A **107**, 2934 (2003).
[3] F. Aguilera-Granja, J. M. Montejano-Carrizalez, and R. A. Guirado-Lopez, Phys. Rev. B **73**, 115422 (2006).
[4] L.-L. Wang and D. D. Johnson, Phys. Rev. B **75**, 235405 (2007).
[5] T. Pawluk, Y. Hirata, and L. Wang, J. Phys. Chem. B **109**, 20817 (2005).
[6] W. Zhang, L. Xiao, Y. Hirata, T. Pawluk, and L. Wang, Chem. Phys. Lett. **383**, 67 (2004).
[7] J. Wang, Phys. Rev. B **75**, 155422 (2007).
[8] P. Bobadova-Parvanova, K. A. Jackson, S. Srinivas, and M. Horoi, Phys. Rev. B **66**, 195402 (2002).
[9] Y. C. Bae, V. Kumar, H. Osanai, and Y. Kawazoe, Phys. Rev. B **72**, 125427 (2005).
[10] Y. C. Bae, H. Osanai, V. Kumar, and Y. Kawazoe, Phys. Rev. B **70**, 195413 (2004).
[11] Deng Kaiming, Yang Jinlong, Xiao Chuanyun, and Wang Kelin, Phys. Rev. B **54**, 2191 (1996).
[12] W. Zhang, H. Zhao, and L. Wang, J. Phys. Chem. B **108**, 2140 (2004).
[13] M. N. Huda, M. K. Niranjan, B. R. Sahu, and L. Kleinman, Phys. Rev. A **73**, 053201 (2006).
[14] A. Nie, J. Wu, C. Zhou, S. Yao, C. Luo, R. C. Forrey, and H. Cheng, Int. J. Quantum Chem. **107**, 219 (2007).
[15] C. M. Chang and M. Y. Chou, Phys. Rev. Lett. **93**, 133401 (2004).
[16] R. C. Longo and L. J. Gallego, Phys. Rev. B **74**, 193409 (2006).
[17] N. Jakse, O. LeBacq, and A. Pasturel, Phys. Rev. B **70**, 174203 (2004).
[18] M. A. Watzky and R. G. Finke, Chem. Mater. **9**, 3083 (1997).
[19] M. B. Knickelbein, Phys. Rev. B **71**, 184442 (2005).
[20] A. J. Cox, J. G. Louderback, S. E. Apsel, and L. A. Bloomfield, Phys. Rev. B **49**, 12295 (1994).
[21] A. J. Cox, J. G. Louderback, and L. A. Bloomfield, Phys. Rev. Lett. **71**, 923 (1993).
[22] X. Liu, M. Bauer, H. Bertagnolli, E. Roduner, J. van Slageren, and F. Phillipp, Phys. Rev. Lett. **97**, 253401 (2006).
[23] M. Sakurai, K. Watanabe, K. Sumiyama, and K. Suzuki, J. Chem. Phys. **111**, 235 (1999).
[24] W. Eberhardt, Surf. Sci. **500**, 242 (2002).
[25] R. G. Parr and W. Yang, *Density-Functional Theory of Atoms and Molecules* (Oxford University Press, New York, 1989).
[26] J. P. Perdew, K. Burke, and M. Ernzerhof, Phys. Rev. Lett. **77**, 3865 (1996).
[27] R. Fournier, J. B. Y. Cheng, and A. Wong, J. Chem. Phys. **119**, 9444 (2003).
[28] H. K. Yuan, H. Chen, A. L. Kuang, A. S. Ahmed, and Z. H. Xiong, Phys. Rev. B **75**, 174412 (2007).
[29] J. Rogan, G. García, C. Loyola, W. Orellana, R. Ramírez, and M. Kiwi, J. Chem. Phys. **125**, 214708 (2006).
[30] R. Fournier, J. Chem. Theory Comput. **3**, 921 (2007).
[31] F. Baletto and R. Ferrando, Rev. Mod. Phys. **77**, 371 (2005).
[32] A. Sebetci and Z. B. Güvenç, Surf. Sci. **525**, 66 (2003).
[33] A. Jiang, T. A. Tyson, and L. Axe, J. Phys.: Condens. Matter **17**, 6111 (2005).
[34] M. S. Daw and M. I. Baskes, Phys. Rev. B **29**, 6443 (1984).
[35] F. Ercolessi, M. Parrinello, and E. Tosatti, Philos. Mag. A **58**, 213 (1988).
[36] A. P. Sutton and J. Chen, Philos. Mag. Lett. **61**, 139 (1990).
[37] J. P. K. Doye and D. J. Wales, J. Chem. Soc., Faraday Trans. **93**, 4233 (1997).
[38] J. P. K. Doye and D. J. Wales, Phys. Rev. Lett. **86**, 5719 (2001).
[39] G. Kresse and J. Furthmüller, Comput. Mater. Sci. **6**, 15 (1996).
[40] G. Kresse and J. Furthmüller, Phys. Rev. B **54**, 11169 (1996).
[41] P. E. Blöchl, Phys. Rev. B **50**, 17953 (1994).
[42] G. Kresse and D. Joubert, Phys. Rev. B **59**, 1758 (1999).

[43] M. Methfessel and A. T. Paxton, Phys. Rev. B **40**, 3616 (1989).
[44] S. Kirkpatrick, C. D. Gelatt, and M. P. Vecchi, Science **220**, 671 (1983).
[45] E. H. L. Aarts and J. Korst, *Simulated Annealing and Boltzmann Machines: A Stochastic Approach to Combinatorial Optimization and Neural Computing* (Wiley, Chichester, UK, 1989).
[46] J. Cheng and R. Fournier, Theor. Chem. Acc. **112**, 7 (2004).
[47] S. Geman and D. Geman, IEEE Trans. Pattern Anal. Mach. Intell. **6**, 721 (1984).
[48] Y. Sun, M. Zhang, and R. Fournier, Phys. Rev. B **77**, 075435 (2008).
[49] See EPAPS Document No. E-PLRAAN-79-114903 for the Cartesian coordinates of the 68 structures and the *s*, *p*, and *d* projected DOS of the six GM clusters. For more information on EPAPS, see http://www.aip.org/pubservs/epaps.html.
[50] S. H. Vosko, L. Wilk, and M. Nusair, Can. J. Phys. **58**, 1200 (1980).
[51] P. Hohenberg and W. Kohn, Phys. Rev. **136**, B864 (1964).
[52] W. Kohn and L. J. Sham, Phys. Rev. **140**, A1133 (1965).
[53] J. C. Slater, *The Self-Consistent Field for Molecules and Solids*, Quantum Theory of Molecules and Solids Vol. 4 (McGraw-Hill, New York, 1974).
[54] D. A. McQuarrie, *Statistical Mechanics* (Harper & Row, New York, 1976).
[55] F. Weinhold, in *Encyclopedia of Computational Chemistry*, edited by P. v. R. Schleyer, P. R. Schreiner, N. L. Allinger, T. Clark, J. Gasteiger, P. Kollman, and H. F. Schaefer III (Wiley, Chichester, UK, 1998), Vol. 3, p. 1792.
[56] B. S. Everitt, S. Landau, and M. Leese, *Cluster Analysis*, 4th ed. (Oxford University Press, New York, 2001).
[57] SAS Institute, *SAS/STAT 9.1 User's Guide* (SAS, Cary, NC, 2004).
[58] SHARCNET, www.sharcnet.ca